
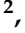






## Article

# Obtaining Polysaccharide-Based Fabrics with Improved Moisture Sorption and Dye Adsorption Properties

Aleksandra Ivanovska <sup>1,\*</sup>, Marija Milošević <sup>2</sup>, Jelena Lađarević <sup>2</sup>, Leposava Pavun <sup>3</sup>, Zorica Svirčev <sup>4,5</sup>,  
Mirjana Kostić <sup>2</sup> and Jussi Meriluoto <sup>4,5,\*</sup>

<sup>1</sup> Innovation Center of the Faculty of Technology and Metallurgy, University of Belgrade, 11120 Belgrade, Serbia

<sup>2</sup> Faculty of Technology and Metallurgy, University of Belgrade, 11120 Belgrade, Serbia

<sup>3</sup> Faculty of Pharmacy, University of Belgrade, 11221 Belgrade, Serbia

<sup>4</sup> Department of Biology and Ecology, Faculty of Sciences, University of Novi Sad, 21000 Novi Sad, Serbia

<sup>5</sup> Faculty of Science and Engineering, Biochemistry, Åbo Akademi University, 20520 Turku, Finland

\* Correspondence: aivanovska@tmf.bg.ac.rs (A.I.); jussi.meriluoto@abo.fi (J.M.); Tel.: +38-11-1330-3628 (A.I.); +35-84-0041-8720 (J.M.)

**Featured Application:** This work has a potential application in biocarpet engineering, which involves the use of cyanobacterial crusts either in the rehabilitation of damaged land surfaces or to combat desertification. Attempts to apply cyanobacterial crusts have not been completely successful so far because the growth of the initial inoculum requires more moisture than arid and semiarid environments can provide. To accelerate the development of the inoculum, it is necessary to provide additional moisture for the growth of cyanobacterial cells. Controlled water delivery could be achieved by using moisture-retentive material that is applied together with the inoculum in the treatment of damaged surfaces. Biocarpet engineering has the potential to solve not only some problems of damaged surfaces and desertification but also reduce and prevent air and water pollution caused by erosion.

**Abstract:** Raw jute fabric was treated with 0.5, 1.0, or 2.0% chitosan solution to improve its sorption properties (evaluated through the moisture sorption and adsorption of textile dye Reactive Orange 16 (RO 16)), which are essential for fabric utilization as geo-prebiotic polysaccharide support that should provide the necessary water for the growth of cyanobacterial communities in biocarpet engineering. Chitosan-treated fabrics possessed 39–78% higher moisture sorption values than the untreated ones. Concerning the dye adsorption, with the increase in its initial concentration, the adsorption potential of raw and fabrics treated with 0.5 or 1.0% chitosan solution was increased up to 1.9 times. The dye adsorption onto these fabrics was exothermic and enthalpy driven. By increasing the chitosan solution percentage up to 1.0%, fabric adsorption potential increased up to 2.2 times. An inverse relationship was observed in the case of the fabric treated with 2.0% chitosan solution, its adsorption potential decreased with increasing the initial dye concentration and temperature due to the different dominant binding interactions. Concerning the contact time, dye adsorption onto fabric treated with 1.0% chitosan solution was rapid in the first 2 h, while the equilibrium was attained after 4.5 h. The isotherm and kinetic data were represented by the Langmuir model and the pseudo-second-order kinetic model, respectively.

**Keywords:** polysaccharide-based fabric; jute; chitosan; adsorption; Reactive Orange 16; Langmuir isotherm; pseudo-second order; adsorption mechanism; restoration of degraded lands and substrates; cyanobacteria



**Citation:** Ivanovska, A.; Milošević, M.; Lađarević, J.; Pavun, L.; Svirčev, Z.; Kostić, M.; Meriluoto, J. Obtaining Polysaccharide-Based Fabrics with Improved Moisture Sorption and Dye Adsorption Properties. *Appl. Sci.* **2023**, *13*, 2512. <https://doi.org/10.3390/app13042512>

Academic Editor: Maria Gavrilescu

Received: 29 January 2023

Revised: 9 February 2023

Accepted: 13 February 2023

Published: 15 February 2023



**Copyright:** © 2023 by the authors. Licensee MDPI, Basel, Switzerland. This article is an open access article distributed under the terms and conditions of the Creative Commons Attribution (CC BY) license (<https://creativecommons.org/licenses/by/4.0/>).

## 1. Introduction

Land degradation is a naturally occurring or human-induced process that affects the functionality of a land ecosystem. More than 40% of terrestrial ecosystems worldwide

(mostly drylands) face significant anthropogenic degradation causing a loss of ecosystem integrity and services, and deterioration of socioeconomic value [1]. The use of induced biological soil crusts (biocrusts) has been advocated in land restoration [2]. The biocrusts consist of complex communities of microorganisms, including cyanobacteria, that live on the top of and in the soil surface. They perform several essential ecosystem functions [3]. Although some research has been invested into restoration by biocrusts, the optimal approach is still to be found [2,4,5].

A field study showed that complex biocrusts, after artificial cyanobacterial inoculation on the sand, were developed within seven years [6], but in some other cases, the process has taken much longer [7]. Therefore, special attention should be paid to the acceleration of biocrust development and succession through the promotion of inoculum viability, for instance, by improving water availability, a key limiting factor. Methods promoting the inoculum/biocrust survival by habitat modification (i.e., improving water retention, reducing UV effects, increasing relative humidity) and leading to a higher growth rate of biocrusts are needed. Based on the results of previous research activities, partially described by the BLOCDUST hypothesis [8,9], it could be supposed that biocrust inoculum survival and efficiency of biocrust restoration could be improved by careful selection of cyanobacterial strains for specific substrates and tailoring geo-prebiotic polysaccharide supports to promote a sustainable relationship between the microbiota and abiotic constituents on the degraded land surface.

For this reason, we decided to prepare polysaccharide-based fabrics with improved sorption properties that were evaluated through the determination of moisture sorption and textile dye adsorption. Among many natural fibers, jute is chosen since this cheap fiber represents the second most important natural fiber (after cotton). The most widespread applications of jute fibers are for the production of packaging materials for agricultural commodities and carpet backings [10]. However, one of the main concerns of both industries is a large amount of jute waste in the form of fabric. This raises the idea of revaluing the discarded jute fabric waste as a valuable polysaccharide-based support. It has to be emphasized that the presence of additional polysaccharides is essential for improving the jute fabric sorption properties and providing the necessary water for the growth of the microbiota. Chitosan as a cheap, biodegradable, biocompatible, nontoxic, and environmental-friendly amino polysaccharide with multifunctional properties [11] might be a good choice for enhancing the sorption properties of raw jute fabric. Many reasons stand behind the decision to select this polysaccharide, whereas the main one is a high affinity between the jute fiber main component, cellulose, and chitosan, which comes from their similar chemical and molecular structures. Additionally, the aldehyde and carboxyl groups present primarily in jute fiber non-cellulosic constituents have an affinity for binding with chitosan.

In this paper, raw jute fabric was treated with different concentrations of chitosan solution to improve its sorption properties. The polysaccharide-based fabrics were characterized using ATR-FTIR spectroscopy and electrokinetic measurements. Their sorption properties were evaluated through the determination of moisture sorption and the adsorption of textile dye Reactive Orange 16, which is used as an indicator for the fabrics' capability to interact with different molecules participating in different interaction mechanisms. The performances of examined fabrics were rated by measuring the adsorption of Reactive Orange 16 vs. initial solution pH, adsorbent mass, initial dye concentration, temperature, and contact time. In addition, equilibrium, kinetic, and thermodynamic studies were performed to establish the most favorable conditions for dye adsorption. The economic impact of the proposed approach can be considered beneficial for possible real application of polysaccharide-based supports since the associated costs are very low. Jute can be used as waste material from the packaging industry, while low-cost chitosan is used at very low concentrations (up to 2.0%).

## 2. Materials and Methods

### 2.1. Material

Raw jute fabric obtained from a commercial supplier (Dekoteks Trade, Belgrade, Serbia) with the following chemical composition: 2.45% water solubles, 0.68% fats and waxes, 1.82% pectin, 13.68% lignin, 16.82% hemicelluloses, and 64.53%  $\alpha$ -cellulose was used in this experiment. All chemicals were p.a. grade and used as received.

### 2.2. Jute Fabric Treatment with Chitosan

Raw jute fabric was washed with distilled water at boiling temperature for 30 min, squeezed, and dipped into 0.5, 1.0, or 2.0% chitosan (low molecular weight chitosan, 50,000–190,000 Da, 75–85% deacetylated, Sigma-Aldrich, Burlington, MA, USA) solution, a material-to-liquid ratio of 1:20. Chitosan dissolution was carried out according to the method described in the literature [12]. After the treatment with chitosan at 60 °C under constant shaking (Memmert, WNE 14, Büchenbach, Germany) for 60 min, fabrics were washed with distilled water, dried in an oven for 30 min at 60 °C, and thereafter at ambient temperature. Raw jute fabric was denoted as J, while chitosan-treated fabrics were marked in accordance with the used chitosan solution concentration, J0.5% CS, J1.0% CS, and J2.0% CS.

### 2.3. Fabrics' Surface Chemistry Characterization

ATR-FTIR spectroscopy (Nicolet™ iS™ 10 FT-IR, Thermo Fisher 2 SCIENTIFIC, Waltham, MA, USA) spectrometer with Smart iTR™ Attenuated Total Reflectance (ATR) Sampling accessory) was used for assessing the changes that occurred in the fabric surface chemistry after the chitosan treatment. The spectra were recorded in the range of 4000–600  $\text{cm}^{-1}$  with 32 scans per spectrum.

The jute fabrics' zeta potential as a function of pH was determined by a streaming potential method using a SurPASS electrokinetic analyzer (Anton Paar GmbH, Graz, Austria) according to the procedure described by Ivanovska et al. [13].

### 2.4. Determination of the Moisture Sorption

Fabrics' moisture sorption was determined by using an Infrared Moisture Analyzer MA 35 (Sartorius, Goettingen, Germany), which continuously monitors the drying process (at 105 °C), stops the measurement when the sample has reached a constant weight (the reproducibility of the weighing system is  $\pm 0.2\%$ ), and automatically calculates its moisture sorption. Before the moisture sorption measurement, fabrics were conditioned according to the procedure described in the literature [14]. The presented results are an average of three measurements per sample.

### 2.5. Dye Adsorption Experiments

An appropriate mass of raw and chitosan-treated jute fabrics was immersed in 100 mL of Reactive Orange 16 (RO 16) (Figure 1) aqueous solution and constantly shaken in the mentioned water bath. The optimization of RO 16 adsorption was done in two steps. First step included optimization of the initial solution pH:  $c_0 = 25 \text{ mg/L}$ ,  $t = 21 \text{ h}$ ,  $T = 25 \text{ °C}$ , adsorbent mass of 0.50 g,  $\text{pH} = 2\text{--}7$ . The second step included optimization of adsorbent mass:  $c_0 = 25 \text{ mg/L}$ ,  $t = 21 \text{ h}$ ,  $T = 25 \text{ °C}$ ,  $\text{pH} = 2$  for fabrics J, J0.5% CS, and J1.0% CS or  $\text{pH} = 4$  for fabric J2.0% CS, an adsorbent mass of 0.25, 0.50, 0.75, or 1.00 g.

Dye removal ( $R$ ) by studied fabrics was calculated by using Equation (1):

$$R (\%) = \frac{A_0 - A_t}{A_0} \cdot 100 \quad (1)$$

where:  $A_0$  and  $A_t$  are the absorbances of the initial dye solution and the dye solution after a certain time, respectively.

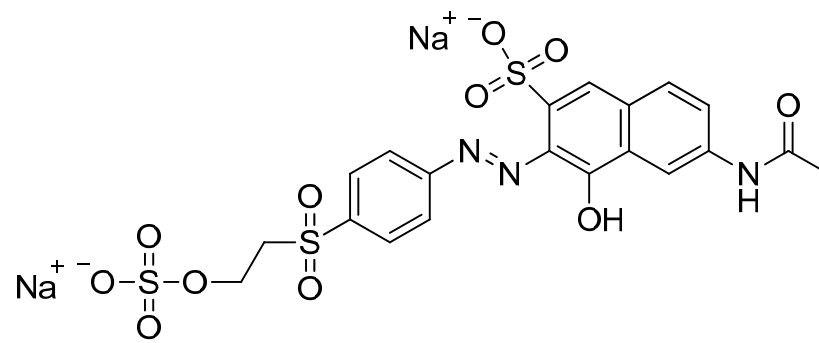


Figure 1. Structure of RO 16.

The fabric adsorption potential, i.e., the mass of dye adsorbed per gram of adsorbent ( $q$ , mg/g), was calculated using Equation (2):

$$q \text{ (mg/g)} = \frac{c_0 - c_t}{m} \cdot V \quad (2)$$

where:  $c_0$  and  $c_t$  (mg/L) are the initial dye concentrations in the solution and in the solution after a certain time, respectively,  $m$  (g) is the adsorbent mass,  $V$  (L) is the solution volume.

The RO 16 concentration in the aqueous solution was determined based on the UV-Vis Shimadzu 1700 spectrophotometer (Shimadzu, Kyoto, Japan) absorbance spectra at  $\lambda_{\max} = 493$  nm. The presented results are the mean values of three measurements per sample whereby the coefficients of variation were below 2.04%.

After finishing the optimization, isotherm, thermodynamic, and kinetic experiments were done under the conditions shown in Figure 2. The obtained data were further modeled using well-known models.

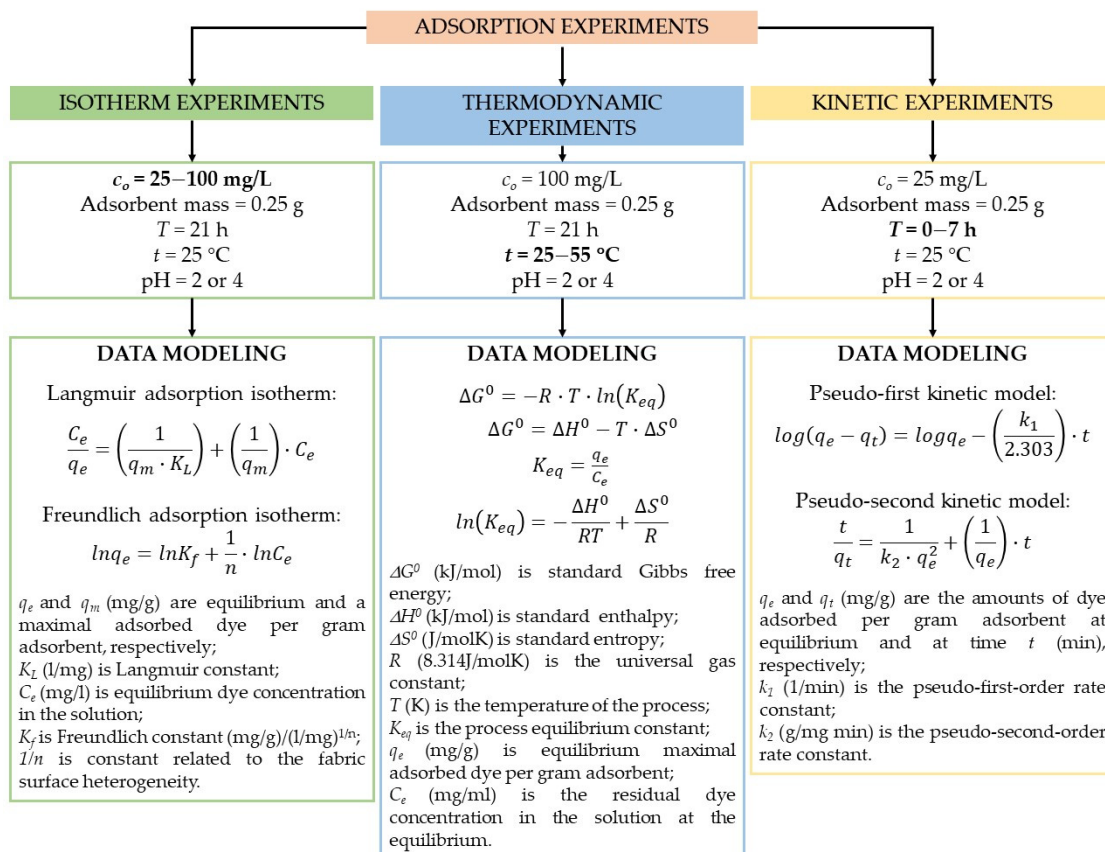
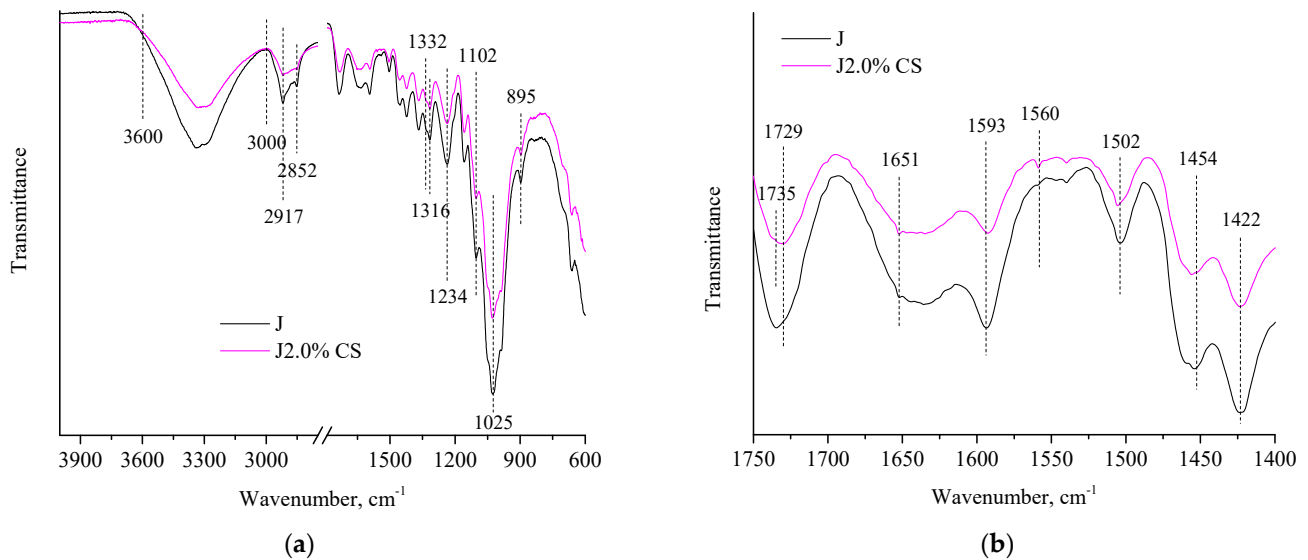


Figure 2. Schematic representation of adsorption experiments and modeling of the obtained data.

### 3. Results and Discussion

#### 3.1. Characterization of Raw and Chitosan Treated Fabrics' Surface Chemistry

The ATR-FTIR spectroscopy was used to characterize the fabrics' surface chemistry and to assess the changes that occurred due to the treatment with chitosan solution. The spectra of J and J2.0% CS (chosen as a representative of chitosan-treated fabrics) show typical bands corresponding to jute fiber main constituents and chitosan (Figure 3).



**Figure 3.** ATR-FTIR spectra of selected fabrics in the range: (a) 4000–600  $\text{cm}^{-1}$  and (b) 1750–1400  $\text{cm}^{-1}$ .

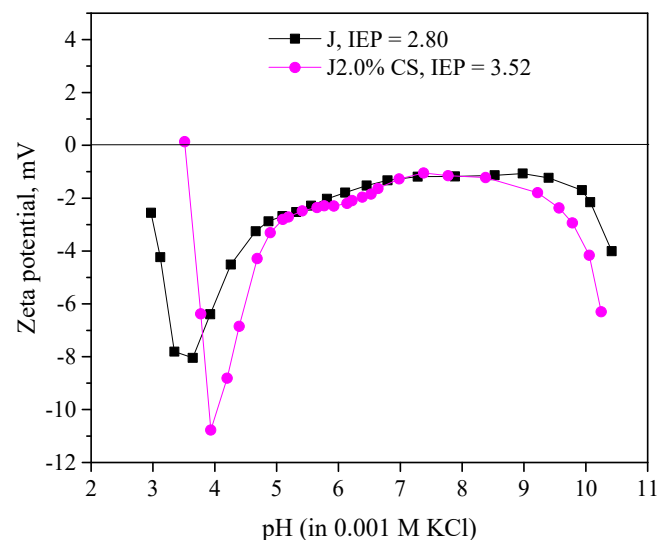
Considering both spectra in parallel, it is evident that the major chitosan band at 1560  $\text{cm}^{-1}$  (related to stretching vibration of its  $-\text{NH}_2$  groups, [12]) appeared, while that at 1651  $\text{cm}^{-1}$  (corresponding to amide I overlapped with  $-\text{OH}$  bending of adsorbed water [15]), it become intensified after the treatment with 2.0% chitosan solution, Figure 3b. The formation of the intermolecular hydrogen bonds between the jute hydroxyl groups (present in cellulose) and chitosan was confirmed by the decreased intensity of the broad-band between 3000–3600  $\text{cm}^{-1}$  assigned to  $-\text{O}-\text{H}$  stretching vibrations overlapped with chitosan  $-\text{NH}_2$  stretching [16], Figure 3a. Furthermore, a high-intensity band at 1735  $\text{cm}^{-1}$  originating from  $-\text{C}=\text{O}$  stretching vibration of carboxyl groups or ester groups present in hemicelluloses [17], as well as aldehyde groups, can be observed in the spectra of raw jute fabric (J). Relocation of the mentioned band to lower wavenumber (1729  $\text{cm}^{-1}$ ) and a significant decrease in its intensity suggest the formation of Schiff base between jute aldehyde groups and chitosan  $-\text{NH}_2$  groups to some extent [18]. In brief, the deposition of the chitosan onto jute fabric could be ascribed to the different mechanisms involving interactions, such as ionic and hydrogen bonding, further supported by the cross-linking of the chains through the chemical bondings to form Schiff bases.

Besides jute fiber groups that participate in the chitosan binding, it should be mentioned that the ATR-FTIR spectra of J and J2.0% CS showed bands originating from cellulose, hemicelluloses, and lignin as the main jute fiber constituents. They are also presented in Figure 3 and summarized in Table 1.

**Table 1.** Wavenumber of IR absorption bands and their interpretation according to the literature [19–25].

Wavenumber, $\text{cm}^{-1}$	Interpretation	Origin
2917, 2852	C–H stretching vibration of $\text{CH}_2$ and CH groups	cellulose and hemicelluloses
1332, 1316, 1102	fingerprint region	polysaccharides, especially cellulose
1025	C–O stretching bond structure	alcohol's functional group
1593, 1422	aromatic skeletal vibrations and ring breathing with C–O stretching	lignin
1502, 1454	aromatic ring C = C of the phenylpropane group	
1234	ring breathing of guaiacyl "G"	
895	$\beta$ -glycosidic linkages between the glycosidic units	cellulose

The previously discussed changes in the fabrics' surface chemistry caused by chitosan treatment should undoubtedly affect their surface charge. Therefore, electrokinetic measurements were done (Figure 4) to give information about the fabric surface charge as a function of pH and indirectly about surface acidic-base functional groups and their reactivity in an aqueous medium [26]. Exactly, the fabric surface charge represents a key parameter responsible for dye adsorption, which is chosen as an indicator for polysaccharide-based fabrics' sorption properties. The results presented in Figure 4 revealed that after the treatment with chitosan, the pH vs. zeta potential curve was shifted to higher pH values and the fabric isoelectric point (IEP) was shifted from 2.80 to 3.52 due to the incorporation of positively charged chitosan  $-\text{NH}_3^+$  groups (since  $-\text{NH}_2$  groups of chitosan are protonated in acidic medium).

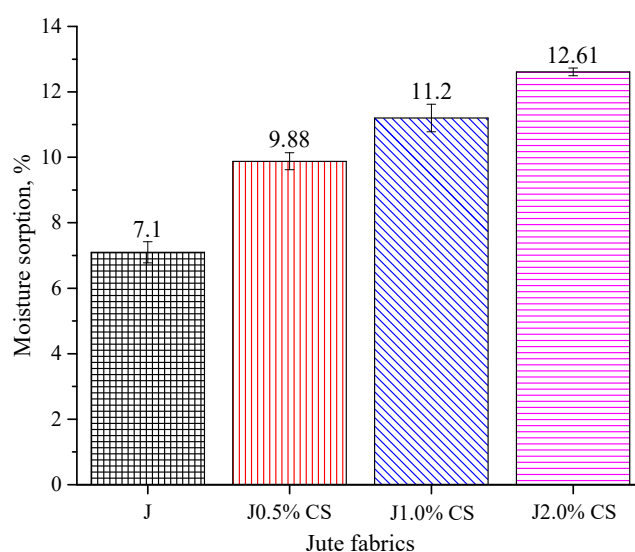
**Figure 4.** Zeta potential and isoelectric points (IEP) of J and J2.0% CS.

The successful functionalization of jute fabrics with chitosan was confirmed through the notable changes observed in the fabric surface chemistry and electrokinetic properties.

### 3.2. Moisture Sorption

Moisture sorption (Figure 5) was studied as one of the essential sorption properties which are of great importance for the utilization of chitosan-treated jute fabrics as water-binding geo-prebiotic polysaccharide supports. Theoretically, the moisture sorption values provide information about the accessibility of the fibers to water vapor [27]. A high

moisture sorption value of raw jute fabric (J) is due to the presence of hydroxyl groups (originating from the main jute constituent, cellulose) that are capable of binding water molecules in the jute fiber amorphous regions as well as on the crystallite surfaces [25]. As the histogram reported, chitosan-treated fabrics J0.5% CS, J1.0% CS, and J2.0% CS possessed 39.2, 57.7, and 77.6% higher moisture sorption ability than J fabric, respectively (Figure 5). Their enhanced moisture sorption can be attributed to the hygroscopic nature of chitosan, i.e., a high ability of its hydroxyl and amino groups to form hydrogen bonds with water [28]. This is additionally supported by the good linear correlation ( $r = 0.985$ ) between the fabric moisture sorption values and chitosan solution concentration used for fabric functionalization.



**Figure 5.** Moisture sorption of raw and chitosan-treated fabrics.

### 3.3. Adsorption of Reactive Orange 16 (RO 16) as an Indicator for Fabric Sorption Properties

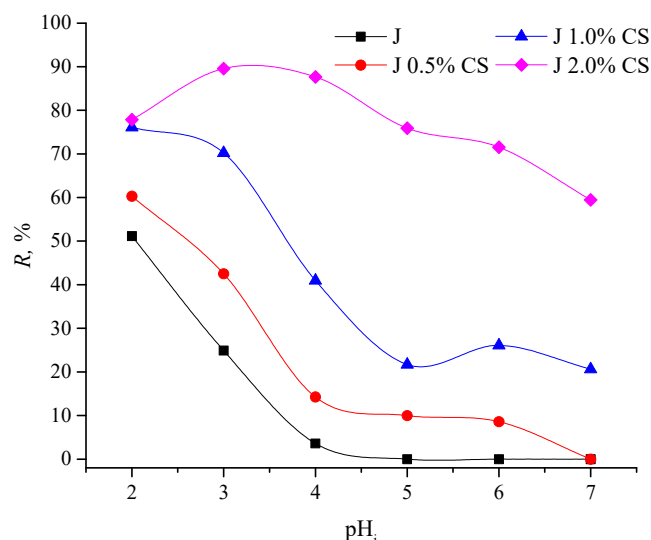
The efficiency of the adsorption of RO 16 onto polysaccharide-based fabrics was studied by varying the following operational parameters: initial solution's pH, adsorbent mass, dye initial concentration, temperature, and contact time. All these experiments were aimed at maximizing the adsorption potential for selected textile dye.

#### 3.3.1. Optimization of the Initial Solution's pH to Achieve Maximum RO 16 Removal

The influence of the initial pH value on the removal/adsorption of RO 16 by different adsorbents was already noted by many authors [29–35]. Therefore, to infer more information about the nature of the adsorption process, the removal (in further text:  $R$ ) of RO 16 by polysaccharide-based fabrics was studied in the pH range of 2–7 by adding appropriate amounts of 1 M HCl, or 0.1 M NaOH. As Figure 6 demonstrates,  $R$  of RO 16 by J, J0.5% CS, J1.0% CS is the highest (accounted by about 51, 60, and 76%, respectively) at a pH 2. Moreover, for fabric J2.0% CS, it can be stated that an optimal solution pH is 4 since there is no significant difference between the  $R$  of dye at a pH 3 and 4 (89.6 vs. 87.6%, Figure 6), and, additionally, the solution's pH 4 is easier to adjust since the lower amount of HCl needs to be added.

Since RO 16 belongs to the class of anionic dyes and is negatively charged in the investigated pH range (2–7), it should be emphasized that different adsorption patterns of raw and chitosan-treated jute fabrics originate solely from the changes on the adsorbent surface caused either by the pH change or chitosan deposition. Firstly, the adsorption of the untreated jute fabric should be taken into account. According to the zeta potential measurements, the isoelectric point (IEP) of J is 2.80, indicating that at  $\text{pH} < 2.80$  its surface is positively charged, while above this value, the adsorbent surface converts to negative. As the maximal adsorption for J is attained at  $\text{pH} = 2$ , it could be suggested that the

adsorption is mainly governed by the electrostatic attraction between negatively charged dye molecules and the positive jute surface. Considering that the molecular structure of RO 16 bears numerous functional groups (Figure 1), it can be supposed that electrostatic interactions are strengthened by multiple hydrogen bonds between dye and fabric surface functional groups, wherein dye can act both as a donor (secondary amino or hydroxyl groups) or acceptor (oxygen of the sulfone, sulfonyl, and carbonyl groups or nitrogen of azo bridge) of hydrogen bonds. Nevertheless, interactions with the lignin portion of jute fabric should not be ruled out since this polymer bears aromatic rings able to interact with the electron-rich phenyl and naphthyl groups of RO 16 via  $\pi$ - $\pi$  stacking interactions [36,37].



**Figure 6.** The impact of the solution's initial pH ( $\text{pH}_i$ ) on the removal ( $R$ ) of RO 16 by different adsorbents ( $c_0 = 25 \text{ mg/L}$ ,  $t = 21 \text{ h}$ ,  $T = 25 \text{ }^\circ\text{C}$ , the adsorbent mass of 0.50 g).

On the other hand, after the chitosan treatment (i.e., chitosan deposition on the jute fabric surface), it is obvious that the  $R$  of RO 16 by the jute fabric is reinforced. For all samples, as discussed above, the optimal  $R$  of RO 16 by J0.5% CS, and J1.0% CS, is also obtained at pH 2, as in the case of J, Figure 6. Promoted adsorption could be related to the increased number of  $\text{NH}_2$  groups introduced with chitosan deposition [38]. These groups are protonated in a highly acidic medium, appearing as ammonium groups ( $\text{NH}_3^+$ ), increasing the electro-positivity of the adsorbent at pH 2, thus offering more active sites for capturing negatively charged dye molecules. Further increase in chitosan concentration ( $-\text{NH}_3^+$  groups) does not bring the enhancement of the dye removal by J1.0% CS and J2.0% CS at pH 2, indicating fabrics' saturation with RO 16 molecules, i.e., there is a definite number of the fabric active sites that could be occupied by large RO 16 molecules. According to Figure 6, it is obvious that in the case of J2.0% CS, governing mechanism that participates in the  $R$  of RO 16 changes, as the optimal  $R$  is achieved approximately at the fabric IEP (between pH 3 and 4, Figure 6). As IEP refers to the pH value for which a number of positively and negatively charged fabric surface groups equals providing a formally neutral surface, the optimal  $R$  of RO 16 by J2.0% CS in a neutral environment is due to a governing mechanism other than electrostatic interactions. The key reason for this lies in the chitosan structure characterized by the abundance of hydroxyl and amino groups and high content of amorphous regions. Increasing the solution pH value causes deprotonation of a certain number of the chitosan ammonium groups and obtaining  $-\text{NH}_2$  groups. Both  $-\text{OH}$  and  $-\text{NH}_2$  groups are able to participate in the effective multiple interactions with the dye molecules, such as hydrogen bonds (dipole-dipole and Yoshida), and  $n$ - $\pi$  stacking interactions between lone pairs of the oxygen and nitrogen atoms and aromatic rings of RO 16 [39–41]. Dipole-dipole hydrogen interactions involve hydrogen atoms of  $-\text{OH}$  and  $-\text{NH}_2$  groups interacting with the oxygen (carbonyl, sulfone, or sulfonyl groups) and

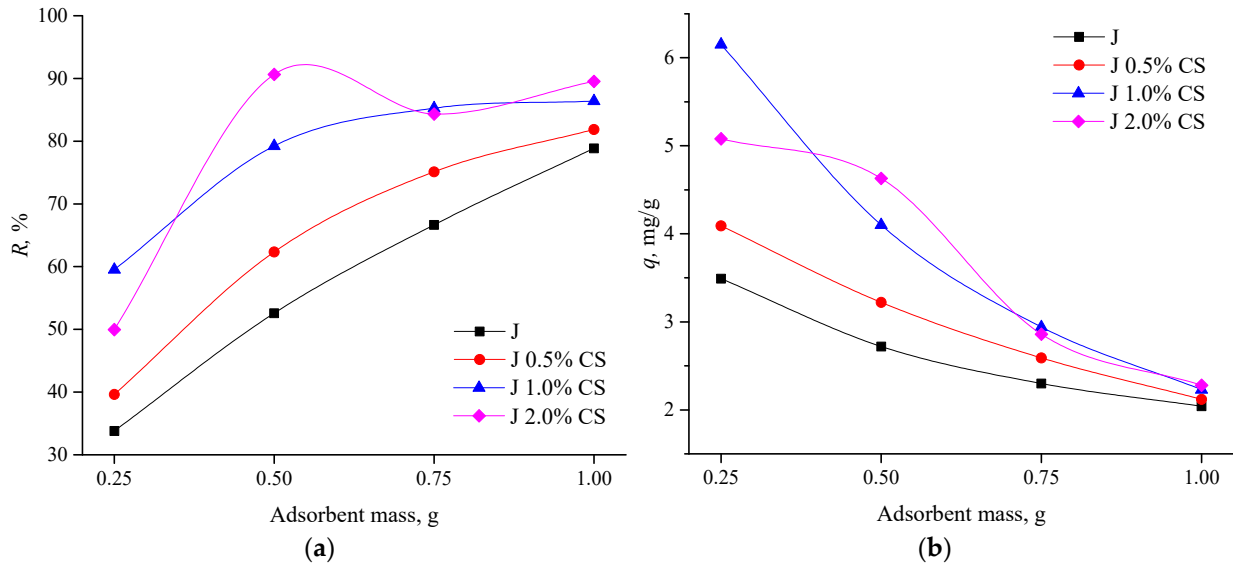


nitrogen atoms (azo bridge), while Yoshida hydrogen bonding includes interactions of hydrogen with RO 16 aromatic rings. Furthermore, the higher  $R$  of RO 16 by J2.0% CS with respect to other adsorbents could also be ascribed to the higher content of amorphous regions present on its surface originating from chitosan that facilitates the trapping of dye molecules.

Further, an increase in the solution pH value causes the decline of the dye removal for all samples since the adsorbent surface becomes neutralized and carries an excess negative charge and thereby repelling the anionic dye. Since the  $R$  of RO 16 was found to be highly pH dependent, further experiments were conducted at a pH of 2.0 (for J, J0.5% CS, and J1.0% CS) and 4.0 (for J2.0% CS).

### 3.3.2. Influence of Adsorbent Mass on Dye Removal and Fabrics' Adsorption Potential for RO 16

The effect of adsorbent mass on the  $R$  of RO 16 and fabrics' adsorption potential (in further text:  $q$ ) for the same dye was investigated by putting 100 mL of RO 16 aqueous solution ( $c_0 = 25$  mg/L) in contact with different amounts (0.25, 0.50, 0.75, or 1.00 g) of raw or chitosan treated jute fabrics. The results presented in Figure 7a show that increments of the adsorbent mass (with the exception of J2.0% CS) give rise to an increase in dye  $R$ . The different shape of J2.0% CS curve is the consequence of different dye-binding mechanisms, reflecting different interactions between dye molecules and fabric surface, which is described further. By increasing the adsorbent mass by 4 times (from 0.25 to 1.00 g), the dye  $R$  by J, J0.5% CS, J1.0% CS, and J2.0% CS increased for 2.3, 2.0, 1.4, and 1.8 times, respectively. This behavior is expected since, with increasing the adsorbent mass, there is a higher number of available adsorption sites capable of interacting with RO 16, leading to the augmentation in the extent of dye removal [42,43].



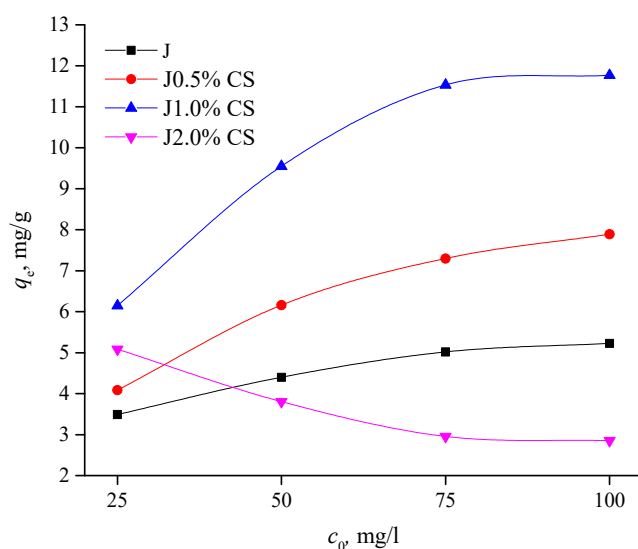
**Figure 7.** The effect of adsorbent mass on: (a) RO 16 removal ( $R$ ) and (b) adsorption potential ( $q$ ) of studied adsorbents ( $c_0 = 25$  mg/L,  $t = 21$  h,  $T = 25$  °C, pH of 2.0 (for J, J0.5% CS, and J1.0% CS) and 4.0 (for J2.0% CS), the mass of adsorbent 0.25–1.00 g).

Although the  $R$  of RO 16 increased with increasing the adsorbent mass, the fabrics'  $q$  conversely declined (Figure 7b). This downward trend can be explained by the fact that when larger amounts of adsorbent are used, the fabrics' adsorption sites remain partially unsaturated during the adsorption process in the presence of constant solution volume, resulting in reduced  $q$  [44]. Similar observations for the adsorbent mass vs.  $R$  of RO 16 and adsorbent mass vs.  $q$  have been reported for different lignocellulosic-based adsorbents [29,30,33,45,46].

From Figure 7b, it is apparent that when 0.25 g of J, J0.5% CS, J1.0% CS, or J2.0% CS was immersed in 100 mL of RO 16 aqueous solution, fabrics'  $q$  accounted for 3.49, 4.09, 6.15, and 5.08 mg/g, respectively. Based on the findings of this section, in further experiments, the adsorbent mass of 0.25 g was fixed for effective dye adsorption.

### 3.3.3. Isotherm Experiments

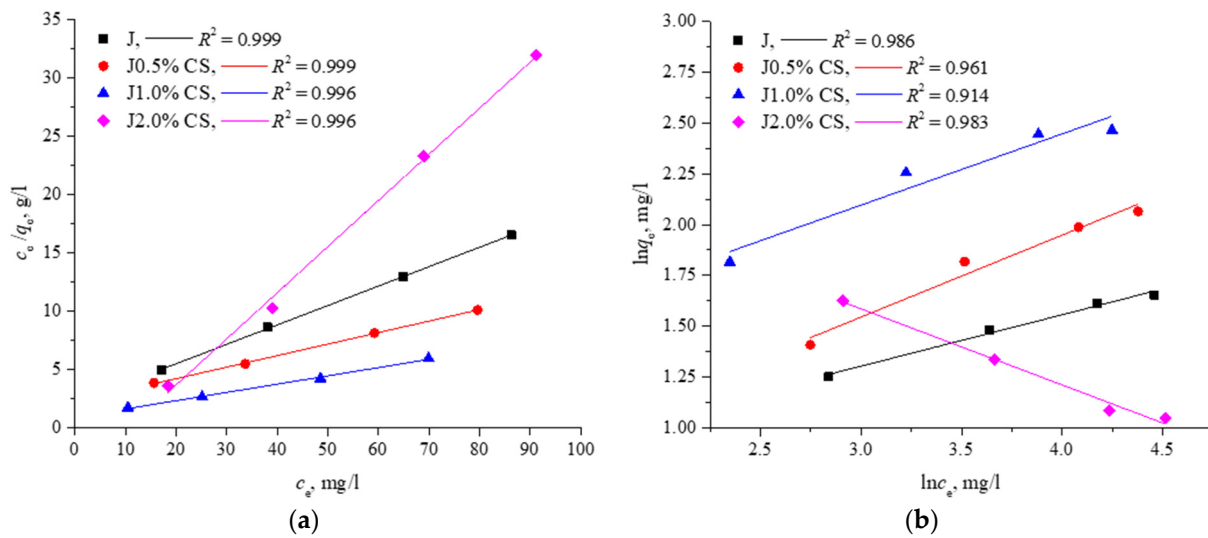
After adopting the previously optimized pH and adsorbent dose, isotherm studies were carried out to gain insights into the distribution of adsorbate at the adsorbent-solution interface [47]. For that purpose, 100 mL of RO 16 aqueous solution of defined concentration (25, 50, 75, or 100 mg/L) was agitated with studied polysaccharide-based fabrics for 21 h. Thereafter, the  $q$  of each fabric was calculated and presented in Figure 8. Obtained results revealed that with the increase in initial RO 16 concentration from 25 to 100 mg/L, the amount of dye adsorbed per gram J, J0.5% CS, or J1.0% CS, increased from 3.49 to 5.22, 4.09 to 7.89, and 6.15 to 11.77 mg/g, respectively. This trend is attributed to the intensified collision among the dye molecules and adsorbent and lower mass transfer resistance at high dye concentrations, both contributing to an increased fabrics'  $q$  [33,48,49]. Unexpectedly, fabric J2.0% CS showed the opposite trend. Its  $q$  decreased from 5.08 down to 2.85 mg/g with increasing the initial RO 16 concentration (Figure 8), which can be attributed to a high mass of chitosan per mass of fabric and governing binding mechanisms other than electrostatic interactions, as it was explained above. It is good to mention that at the initial dye concentration of 50–100 mg/L, among all tested fabrics, the lowest  $q$  is observed for fabric J, which was improved after the treatment with 0.5 or 1.0% chitosan. When the initial dye's concentration was set at 100 mg/L, by increasing the chitosan percentage from 0 to 0.5 and 1.0,  $q$  of J0.5% CS and J1.0% CS increased by 1.5 and 2.2 times, respectively. For both J0.5% CS and J1.0% CS, favorable concave-shaped isotherms without strict plateau were observed, indicating their higher affinity for RO 16 and a saturation trend at high dye concentrations [32].



**Figure 8.** The effect of initial RO 16 concentration ( $c_0$ ) on the adsorption potential ( $q$ ) of raw and chitosan-treated fabrics ( $c_0 = 25, 50, 75$ , or  $100$  mg/L,  $t = 21$  h,  $T = 25$  °C, pH of 2.0 (for J, J0.5% CS, and J1.0% CS) and 4.0 (for J2.0% CS), the mass of adsorbent 0.25 g).

The data presented in Figure 8 were modeled using linearized forms of Langmuir and Freundlich isotherm models (Figure 1), and the isotherm parameters calculated from the intercepts and slopes of the corresponding linear plots (Figure 9) are listed in Table 2. The values of the correlation coefficients ( $R^2$ ) were compared, and it was found that the adsorption of RO 16 onto studied fabrics was better represented by the Langmuir than by the Freundlich isotherm ( $R^2 = 0.996$ – $0.999$  vs.  $0.914$ – $0.986$ ). The applicability of the

Langmuir isotherm model means that the adsorption occurs at specific, energetically equivalent sites of the fabric with monolayer coverage of the dye over a homogeneous adsorbent surface [36]. This model was also found suitable for describing the adsorption of RO 16 onto corn cob [32], ethylenediamine modified rice hull [50], cotton fabric loaded with metal-organic frame material UiO-66 [48], phosphoric acid activated carbon from *Melia azedarach* waste sawdust [29], jute stick activated carbon [33], and waste sunflower seed shells [32].



**Figure 9.** Modeling the isotherm data presented in Figure 8 using: (a) Langmuir and (b) Freundlich isotherm models and the linear fit of experimental data for RO 16 adsorption.

**Table 2.** Isotherm parameters for RO 16 adsorption onto studied adsorbents.

Adsorption Isotherm	Isotherm Parameters	Adsorbents			
		J	J0.5% CS	J1.0% CS	J2.0% CS
Langmuir	$K_L$	0.008	0.044	0.080	−0.093
	$q_m$	5.996	10.128	14.075	2.525
Freundlich	$K_f$	1.719	1.394	2.838	15.035
	$1/n$	0.254	0.404	0.351	−0.375

$K_L$  (L/mg) is Langmuir constant,  $K_f$  (mg/g)/(L/mg)<sup>1/n</sup> is Freundlich constant, and  $1/n$  is a constant related to the fabric surface heterogeneity.

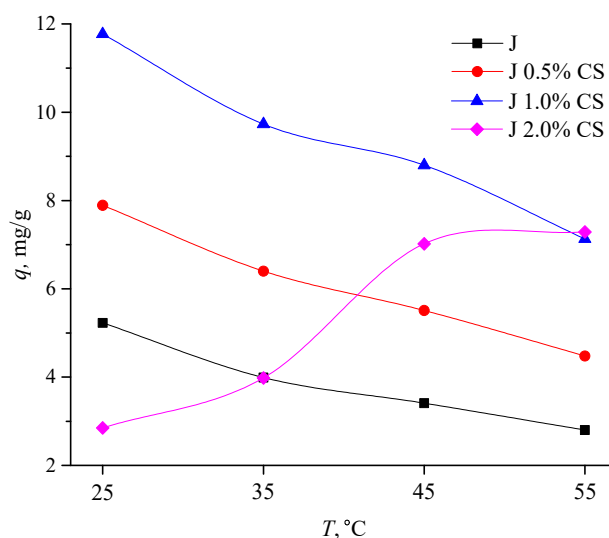
It should not be neglected that the Langmuir model allows the calculation of the Langmuir constant,  $K_L$ , and adsorbent maximum adsorption capacity,  $q_m$  (Table 2). Much higher  $K_L$  values observed for J1.0% CS than for other fabrics suggest a stronger interaction between that fabric and RO 16 than between other fabrics and dye. Furthermore, based on the results listed in Table 2, it is evident that fabrics treated with 0.5 or 1.0% chitosan are characterized by 1.7 or 2.3 times higher  $q_m$  than untreated fabric. The situation is different in the case of J2.0% CS. The theoretical monolayer maximum adsorption capacity of this fabric accounted for 2.525 after the chitosan treatment due to the previously discussed higher content of chitosan on the fabric surface as well as a different binding mechanism.

Parameter  $q_m$  is also very useful for the comparison of the adsorption capacities of different adsorbents for the same dye. Besides the complicated route for obtaining cotton fabric loaded with metal-organic frame material UiO-66, long reaction time (12 h), used toxic DMF, and high operation temperature (80 °C), its  $q_m$  for RO 16 is only 5.17 mg/g [48], which is even lower than that observed for untreated jute (5.996 mg/g, Table 2). Furthermore, although activated carbons studied in the earlier literature [28,33] have higher  $q_m$  for RO 16, they cannot compete with J1.0% CS since during their preparation, high temperatures

and non-environmental friendly chemicals (like 85% ortho-phosphoric acid) were used, raising the question regarding the adsorbent cost-effectiveness. The economic impact of the proposed approach can be considered beneficial for possible real applications since the associated costs are very low because 1.0% of chitosan solution was used for the functionalization of fabric that possessed the highest  $q$  for RO 16.

### 3.3.4. Thermodynamic Studies

It is well known that thermodynamic experiments are important for probing the nature and mechanism of dye adsorption [48], hence, the impact of different temperatures (25, 35, 45, and 55 °C) on RO 16 adsorption onto investigated fabrics was examined. The data shown in Figure 10 point out that temperature has two different effects on the  $q$  of fabrics. Namely, with increasing the temperature from 25 to 55 °C,  $q$  of J, J0.5% CS, and J1.0% CS decreased by about 46, 43, and 39%, respectively. It has been reported that an increase in the temperature beyond an optimum value can lead to the breakdown of weak interaction forces that are involved in the adsorption of the dye onto the adsorbent surface [45]. Interestingly, an inverse relationship between temperature and RO 16 adsorption onto J2.0% CS was observed. A significant increase (156%) in the  $q$  of J2.0% CS with increasing temperature was visible in Figure 10. Similar conclusions were recently drawn by Srikantan et al. [45] and Kheradmand et al. [30] for the adsorption of RO 16 onto sunflower hairy roots, and lignocellulosic biomass waste supported with  $\text{FeCl}_3/\text{Zn}(\text{NO}_3)_2$ , respectively.



**Figure 10.** The influence of temperature ( $T$ ) on the adsorption potential ( $q$ ) of examined fabrics ( $c_0 = 100$  mg/L,  $t = 21$  h,  $T = 25, 35, 45,$  or  $55$  °C, pH of 2.0 (for J, J0.5% CS, and J1.0% CS) and 4.0 (for J2.0% CS), the mass of adsorbent 0.25 g).

The data shown in Figure 10 were used for the calculation of the main thermodynamic parameters that were employed to determine the feasibility, spontaneity, and nature of the adsorption process by means of Gibbs free energy ( $\Delta G^\circ$ ), enthalpy ( $\Delta H^\circ$ ), and entropy ( $\Delta S^\circ$ ), respectively. The values of the calculated thermodynamic parameters are summarized in Table 3. The obtained negative values for  $\Delta G^\circ$  proposed that, in the studied temperature range, the process under examination is spontaneous and thermodynamically feasible [51]. Moreover, the  $\Delta G^\circ$  values ranged between  $-20$  and  $0$  kJ/mol, confirming the weak and physical nature of the interactions between fabrics and RO 16 [52]. In the case of the RO 16 adsorption onto J, J0.5% CS, and J1.0% CS, the process is exothermic, i.e., thermodynamically favored at lower temperatures (as already observed in Figure 10) and enthalpy driven since the negative  $\Delta H^\circ$  and  $\Delta S^\circ$  values were obtained, Table 3. Gradual increase of  $\Delta G^\circ$  value with an increase in the temperature from 298.15 to 328.15 K supports the dominant bonding between RO 16 and J, J0.5% CS, and J1.0% CS as was previously

proven by the Langmuir model [34]. Contrary to the above-discussed, the positive  $\Delta H^\circ$  and  $\Delta S^\circ$  values obtained for J2.0% CS evidenced that the adsorption of RO 16 onto this fabric is of endothermic character and some structurally-based dye-fabric complexes during the adsorption process coupled by an increased state of randomness at the solid/liquid interface [29]. According to Suteu et al. [32], the positive entropy reflects the release of high amounts of water molecules due to the sorption of large hydrated dye anions onto an adsorbent.

**Table 3.** Thermodynamic parameters for RO 16 adsorption onto investigated adsorbents.

Fabric	Temperature, K	Thermodynamic Parameters		
		$\Delta G^\circ$ , kJ/mol	$\Delta H^\circ$ , kJ/mol	$\Delta S^\circ$ , J/mol K
J	298.15	−10.17	−17.80	−25.81
	308.15	−9.73		
	318.15	−9.59		
	328.15	−9.37		
J0.5% CS	298.15	−11.39	−17.16	−19.40
	308.15	−11.12		
	318.15	−11.02		
	328.15	−10.78		
J1.0% CS	298.15	−12.71	−16.43	−12.58
	308.15	−12.47		
	318.15	−12.52		
	328.15	−12.27		
J2.0% CS	298.15	−8.53	32.14	136.52
	308.15	−9.75		
	318.15	−11.82		
	328.15	−12.37		

The key to different RO 16 adsorption behavior depending on temperature lies in the different nature of binding mechanisms of J, J0.5% and J1.0% compared to J2.0% CS. In the case of the RO 16 adsorption onto J, J0.5% CS, and J1.0% CS, electrostatic interactions represent the main driving force for the adsorption, hence the positive charge of the fabric surface is neutralized through the interaction with negative moieties of the dye molecules. As the adsorption is enhanced with the increased number of  $\text{NH}_2$  groups introduced with chitosan deposition, it is clear that the adsorption is followed by the entropy decrease ( $\Delta S^\circ < 0$ ) since the nature of the process leads to a more ordered system, i.e., the randomness of RO 16 binding at the solid-liquid interface decreases.

In contrast, due to the formally neutral charge surface of the J2.0% CS, the adsorption of the RO 16 is established through various interactions other than electrostatic interactions. As a consequence of their diversity, the interactions are established sporadically and irregularly, and the organization of the molecules on the solid-solution interface becomes more random, reflected as a positive value of entropy ( $\Delta S^\circ > 0$ ). In such a way, the negative charges of the dyes are not strictly oriented to neutralize the remaining fabric's  $\text{NH}_3^+$  groups at pH 4 (as in the case of other jute fabrics) but are mainly directed away from the surface towards the solution preventing additional adsorption of the dye molecules through the electrostatic repulsion. As the temperature increases, the kinetic energy of the dyes is higher, they move faster, collide, rotate, and orientate in a more favorable way to reduce repulsion. As a consequence, more effective interactions are established, causing higher adsorption potential at higher temperatures.

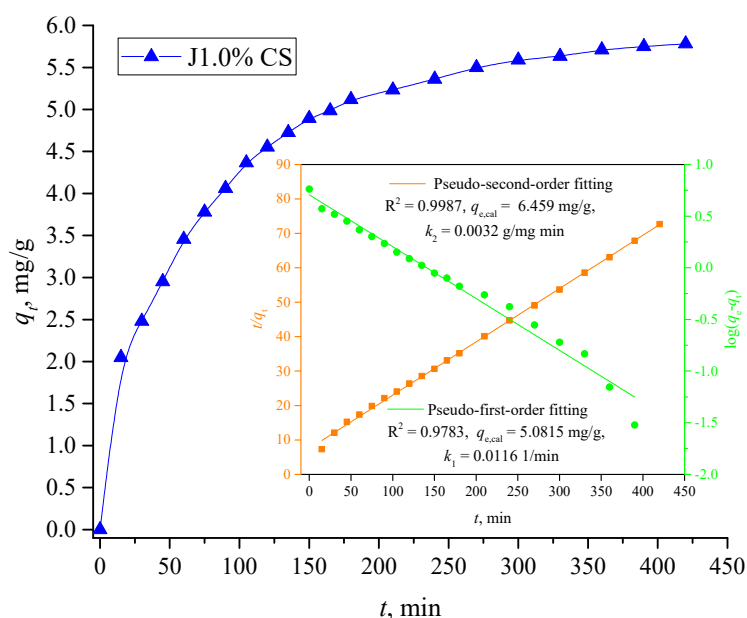
### 3.3.5. Kinetic Experiments

Since the establishment of an adsorption equilibrium is one of the most important aspects while designing an adsorption process, the effect of contact time on the  $q$  of J1.0% CS was investigated. The UV-V absorption spectra of dye solutions were acquired at time

intervals of 15 min up to 3 h and 30 min up to 7 h of contact time, as shown in Figure 11. It is quite evident that the adsorption of RO 16 can be divided into three distinct phases:

- (i) rapid dye adsorption during the first 2 h, adsorption process shows 79% of the equilibrium adsorption capacity of J1.0% CS which is ascribed to a high number of free available sites capable of binding dye molecules;
- (ii) a slower rate of dye adsorption from 2 to 4.5 h reaching about 95% of the adsorbent equilibrium adsorption capacity, an increased competition of dye molecules present in the aqueous phase occurred as a consequence of the fewer available binding sites on the adsorbent surface;
- (iii) dye adsorption becomes negligible in the last stage from 4.5 to 7 h,  $\Delta q_t$  is 4.8%, so it can be stated that equilibrium was reached after 4.5 h of contact time.

The time required for attaining adsorption equilibrium (270 min) is quite similar or shorter when compared to other adsorbents, such as phosphoric acid activated carbon from *Melia azedarach* waste sawdust [29] and waste sunflower seed shells [32].



**Figure 11.** Adsorption of RO 16 onto J1.0% CS as a function of contact time, inset: Pseudo-first and pseudo-second-order kinetic models and calculated kinetic parameters ( $c_0 = 25$  mg/L,  $t = 0$ –7 h,  $T = 25$  °C, pH of 2.0 (for J, J0.5% CS, and J1.0% CS) and 4.0 (for J2.0% CS), the mass of adsorbent 0.25 g).

To explore the kinetics involved in RO 16 adsorption, the experimental data were fitted with pseudo-first-order and pseudo-second-order kinetic models, Figure 1. Higher deviation of  $q_{e,cal}$  from  $q_{e,exp}$  and lower  $R^2$  values were observed for the pseudo-first-order model compared to the pseudo-second-order model ( $\Delta q_e = 11.7\%$  vs.  $12.1\%$ ,  $R^2 = 0.9783$  vs.  $0.9987$ ), inset of Figure 11. It thus appears that the system under study is more appropriately described by the pseudo-second-order model, which is based on the assumption that the rate-limiting step may be chemical sorption or chemisorption involving valency forces through sharing or exchange of electrons between adsorbent and dye [53].

The findings of this section prove that the adsorption of selected dye can be used as an indicator for polysaccharide-based fabrics' sorption properties, as well as their capability to interact with different molecules participating in different interaction mechanisms.

#### 4. Conclusions

Raw jute fabric (J) was treated with 0.5, 1.0, or 2.0% chitosan solution (J0.5% CS, J1.0% CS, and J2.0% CS) to improve its sorption properties which are of great importance for the

utilization of such polysaccharide-based fabrics as water-binding geo-prebiotic supports that should provide the necessary water for the growth of cyanobacterial biocrusts. The fabrics' sorption properties were assessed by the determination of moisture sorption value and their ability to adsorb textile dye Reactive Orange 16 (RO 16). Chitosan-treated jute fabrics possessed up to 77.6% higher moisture sorption values than J, which is owed to the chitosan's greater capability to form hydrogen bonding with water.

On the other hand, after the optimization of RO 16 adsorption in terms of the initial solution's pH (pH 4.0 was found optimal for J2.0% CS, while pH 2.0 was optimal for other fabrics) and adsorbent mass (0.25 g for all fabrics), the effect of dye initial concentration, temperature, and time on fabrics' adsorption potential was investigated. With the increase in initial RO 16 concentration from 25 to 100 mg/L, the amount of dye adsorbed per gram of J, J0.5% CS, and J1.0% CS increased by 1.5, 1.9, and 1.9, times, respectively. Furthermore, by increasing the chitosan percentage from 0 to 0.5, 1.0, fabric adsorption potential increased by 1.5, and 2.2 times (initial dye concentration of 100 mg/L), respectively. The adsorption of RO 16 onto all studied fabrics was represented by the Langmuir isotherm model with a calculated maximum adsorption capacity of 5.996–14.075 mg/g. In the studied temperature range (25 to 55 °C), the adsorption process under examination is spontaneous and thermodynamically feasible. With increasing the temperature to 30 °C, the adsorption potential of J, J0.5% CS, and J1.0% CS decreased by about 46, 33, and 39%, respectively; the adsorption process is exothermic and enthalpy driven. However, an inverse relationship between RO 16 adsorption onto J2.0% CS, initial dye concentration, and temperature was observed. Different behavior of J, J0.5% CS, and J1.0% CS, on one side, and J2.0% CS, on the other side, could be explained by the different dominant binding interactions. In the first case, governing mechanism is ascribed to electrostatic interactions between negatively charged dye and positively charged fabrics' surface, while in the case of J2.0% CS at pH 4, hydrogen bonds and stacking interactions play a major role in the adsorption of RO 16.

Concerning the contact time, adsorption of RO 16 is rapid during the first 2 h, a slower rate of adsorption was observed between 2 and 4.5 h, after which the equilibrium was attained. The kinetic data followed the pseudo-second-order kinetic model.

The findings of this paper confirm that the treatment with chitosan can improve the jute fabric sorption properties. The economic impact of the proposed approach can be considered beneficial for possible real-life applications of polysaccharide-based supports in biocarpet engineering since the associated costs are very low as jute can be obtained as waste material from the packaging industry while the low-cost chitosan was used in very low concentrations (up to 2.0%).

**Author Contributions:** Conceptualization, A.I.; methodology, A.I. and M.M.; formal analysis, A.I. and M.M.; writing—original draft preparation, A.I. and J.L.; writing—review and editing, J.L., L.P., Z.S., M.K. and J.M.; visualization, A.I. and M.M.; supervision, M.K. and J.M.; funding acquisition, Z.S. All authors have read and agreed to the published version of the manuscript.

**Funding:** This research was funded by the Science Fund of the Republic of Serbia, #7726976, Integrated Strategy for Rehabilitation of Disturbed Land Surfaces and Control of Air Pollution-RECAP and Ministry of Education, Science and Technological Development of the Republic of Serbia [Contract No. 451-03-47/2023-01/200287, 451-03-47/2023-01/200135 and 451-03-47/2023-01/200161].

**Institutional Review Board Statement:** Not applicable.

**Informed Consent Statement:** Not applicable.

**Data Availability Statement:** The data presented in this study are available on request from the corresponding author.

**Acknowledgments:** A.I., M.M., Z.S., and M.K. would like to acknowledge financial support from the Science Fund of the Republic of Serbia, #7726976, Integrated Strategy for Rehabilitation of Disturbed Land Surfaces and Control of Air Pollution-RECAP. The authors thank Matea Korica (Innovation Center of the Faculty of Technology and Metallurgy, University of Belgrade) for the measurement of fabric zeta potential.

**Conflicts of Interest:** The authors declare no conflict of interest.

## References

1. Reynolds, J.F.; Stafford Smith, D.M.; Lambin, E.F.; Turner, B.L.; Mortimore, M.; Batterbury, S.P.J.; Downing, T.E.; Dowlatabadi, H.; Fernández, R.J.; Herrick, J.E.; et al. Global desertification: Building a science for dryland development. *Science* **2007**, *316*, 847–851. [[CrossRef](#)] [[PubMed](#)]
2. Chamizo, S.; Mugnai, G.; Rossi, F.; Certini, G.; De Philippis, R. Cyanobacteria inoculation improves soil stability and fertility on different textured soils: Gaining insights for applicability in soil restoration. *Front. Environ. Sci.* **2018**, *6*, 49. [[CrossRef](#)]
3. Rossi, F.; Li, H.; Liu, Y.; De Philippis, R. Cyanobacterial inoculation (cyanobacterisation): Perspectives for the development of a standardized multifunctional technology for soil fertilization and desertification reversal. *Earth-Sci. Rev.* **2017**, *171*, 28–43. [[CrossRef](#)]
4. Antoninka, A.; Faist, A.; Rodriguez-Caballero, E.; Young, K.E.; Chaudhary, V.B.; Condon, L.A.; Pyke, D.A. Biological soil crusts in ecological restoration: Emerging research and perspectives. *Restor. Ecol.* **2020**, *28*, S3–S8. [[CrossRef](#)]
5. Roncero-Ramos, B.; Muñoz-Martín, M.A.; Cantón, Y.; Chamizo, S.; Rodríguez-Caballero, E.; Mateo, P. Land degradation effects on composition of pioneering soil communities: An alternative successional sequence for dryland cyanobacterial biocrusts. *Soil Biol. Biochem.* **2020**, *146*, 107824. [[CrossRef](#)]
6. Wu, Y.; Rao, B.; Wu, P.; Liu, Y.; Li, G.; Li, D. Development of artificially induced biological soil crusts in fields and their effects on top soil. *Plant Soil* **2013**, *370*, 115–124. [[CrossRef](#)]
7. Belnap, J. Recovery rates of cryptobiotic crusts: Inoculant use and assessment methods. *Great Basin Natur.* **1993**, *53*, 89–95.
8. Svirčev, Z.; Marković, S.B.; Stevens, T.; Codd, G.A.; Smalley, I.; Simeunović, J.; Obreht, I.; Dulić, T.; Pantelić, D.; Hambach, U. Importance of biological loess crusts for loess formation in semi-arid environments. *Quat. Int.* **2013**, *296*, 206–215. [[CrossRef](#)]
9. Svirčev, Z.; Dulić, T.; Obreht, I.; Codd, G.A.; Lehmkuhl, F.; Marković, S.B.; Hambach, U.; Meriluoto, J. Cyanobacteria and loess—An underestimated interaction. *Plant Soil* **2019**, *439*, 293–308. [[CrossRef](#)]
10. Ivanovska, A.; Asanović, K.; Jankoska, M.; Pavlović, S.; Poparić, G.; Kostić, M. Alkali treated jute fabrics suitable for the production of inexpensive technical textiles. *Fiber. Polym.* **2022**, *23*, 2306–2315. [[CrossRef](#)]
11. Korica, M.; Peršin, Z.; Trifunović, S.; Mihajlovski, K.; Nikolić, T.; Maletić, S.; Fras Zemljič, L.; Kostić, M.M. Influence of different pretreatments on the antibacterial properties of chitosan functionalized viscose fabric: TEMPO oxidation and coating with TEMPO oxidized cellulose nanofibrils. *Materials* **2019**, *12*, 3144. [[CrossRef](#)]
12. Kramar, A.D.; Ilic-Tomic, T.R.; Lađarević, J.M.; Nikodinovic-Runic, J.B.; Kostic, M.M. Halochromic cellulose textile obtained via dyeing with biocolorant isolated from *Streptomyces sp.* strain NP<sub>4</sub>. *Cellulose* **2021**, *28*, 8771–8784. [[CrossRef](#)]
13. Ivanovska, A.M.; Kostić, M.M. Electrokinetic properties of chemically modified jute fabrics. *J. Serb. Chem. Soc.* **2020**, *85*, 1621–1627. [[CrossRef](#)]
14. Koblyakov, A. *Laboratory Practice in the Study of Textile Materials*, 1st ed.; Mir Publishers: Moscow, Russia, 1989; pp. 192–200.
15. El-Shafei, A.M.; Adel, A.M.; Ibrahim, A.A.; Al-Shemy, M.T. Dual functional jute fabric biocomposite with chitosan and phosphorylated nano-cellulose (antimicrobial and thermal stability). *Int. J. Biol. Macromol.* **2019**, *124*, 733–741. [[CrossRef](#)] [[PubMed](#)]
16. Yang, J.; Kwon, G.-J.; Hwang, K.; Kim, D.-Y. Cellulose-chitosan antibacterial composite films prepared from LiBr solution. *Polymers* **2018**, *10*, 1058. [[CrossRef](#)]
17. Ivanovska, A.; Asanovic, K.; Jankoska, M.; Mihajlovski, K.; Pavun, L.; Kostic, M. Multifunctional jute fabrics obtained by different chemical modifications. *Cellulose* **2020**, *27*, 8485–8502. [[CrossRef](#)]
18. Kim, U.-J.; Lee, Y.R.; Kang, T.H.; Choi, J.W.; Kimura, S.; Wada, M. Protein adsorption of dialdehyde cellulose-crosslinked chitosan with high amino group contents. *Carbohydr. Polym.* **2017**, *163*, 34–42. [[CrossRef](#)]
19. Ivanovska, A.; Milošević, M.; Obradović, B.; Svirčev, Z.; Kostić, M. Plasma treatment as a sustainable method for enhancing the wettability of jute fabrics. *Sustainability* **2023**, *15*, 2125. [[CrossRef](#)]
20. Schwanninger, M.; Rodrigues, J.C.; Pereira, H.; Hinterstoisser, B. Effects of short-time vibratory ball milling on the shape of FT-IR spectra of wood and cellulose. *Vib. Spectrosc.* **2004**, *36*, 23–40. [[CrossRef](#)]
21. Bakri, M.K.B.; Jayamani, E.; Hamdan, S.; Rahman, M.R.; Soon, K.H.; Kakar, A. Fundamental study on the effect of alkaline treatment on natural fibers structures and behaviors. *ARNP J. Eng. Appl. Sci.* **2016**, *11*, 8759–8763.
22. Ivanovska, A.; Veljović, S.; Dojčinović, B.; Tadić, N.; Mihajlovski, K.; Natić, M.; Kostić, M. A strategy to revalue a wood waste for simultaneous cadmium removal and wastewater disinfection. *Adsorpt. Sci. Technol.* **2021**, *2021*, 3552300. [[CrossRef](#)]
23. Ahuja, D.; Kaushik, A.; Chauhan, G.S. Fractionation and physicochemical characterization of lignin from waste jute bags: Effect of process parameters on yield and thermal degradation. *Int. J. Biol. Macromol.* **2017**, *97*, 403–410. [[CrossRef](#)] [[PubMed](#)]
24. Zhang, H.; Ming, R.; Yang, G.; Li, Y.; Li, Q.; Shao, H. Influence of alkali treatment on flax fiber for use as reinforcements in polylactide stereocomplex composites. *Polym. Eng. Sci.* **2015**, *55*, 2553–2558. [[CrossRef](#)]
25. Ivanovska, A.; Cerovic, D.; Maletic, S.; Jankovic Castvan, I.; Asanovic, K.; Kostic, M. Influence of the alkali treatment on the sorption and dielectric properties of woven jute fabric. *Cellulose* **2019**, *26*, 5133–5146. [[CrossRef](#)]
26. Korica, M.; Peršin, Z.; Fras Zemljič, L.; Mihajlovski, K.; Dojčinović, B.; Trifunović, S.; Vesel, A.; Nikolić, T.; Kostić, M.M. Chitosan nanoparticles functionalized viscose fabrics as potentially durable antibacterial medical textiles. *Materials* **2021**, *14*, 3762. [[CrossRef](#)]



27. Kramar, A.; Ivanovska, A.; Kostić, M. Regenerated cellulose fiber functionalization by two-step oxidation using sodium periodate and sodium chlorite—Impact on the structure and sorption properties. *Fibers Polym.* **2021**, *22*, 2177–2186. [[CrossRef](#)]
28. Szymańska, E.; Winnicka, K. Stability of chitosan—A challenge for pharmaceutical and biomedical applications. *Mar. Drugs* **2015**, *13*, 1819–1846. [[CrossRef](#)]
29. Shah, J.A.; Butt, T.A.; Mirza, C.R.; Shaikh, A.J.; Khan, M.S.; Arshad, M.; Riaz, N.; Haroon, H.; Gardazi, S.M.H.; Yaqoob, K.; et al. Phosphoric acid activated carbon from *Melia azedarach* waste sawdust for adsorptive removal of reactive orange 16: Equilibrium modelling and thermodynamic analysis. *Molecules* **2020**, *25*, 2118. [[CrossRef](#)] [[PubMed](#)]
30. Kheradmand, A.; Negarestani, M.; Mollahosseini, A.; Shayesteh, H.; Farimaniraad, H. Low-cost treated lignocellulosic biomass waste supported with FeCl<sub>3</sub>/Zn(NO<sub>3</sub>)<sub>2</sub> for water decolorization. *Sci. Rep.* **2022**, *12*, 16442. [[CrossRef](#)]
31. Ong, S.T.; Lee, C.K.; Zainal, Z. Removal of basic and reactive dyes using ethylenediamine modified rice hull. *Bioresour. Technol.* **2007**, *98*, 2792–2799. [[CrossRef](#)]
32. Suteu, D.; Malutan, T.; Bilba, D. Agricultural waste corn cob as a sorbent for removing reactive dye orange 16: Equilibrium and kinetic study. *Cell. Chem. Technol.* **2011**, *45*, 413–420.
33. Ghosh, R.K.; Ray, D.P.; Tewari, A.; Das, I. Removal of textile dyes from water by jute stick activated carbon: Process optimization and isotherm studies. *Int. J. Environ. Sci. Technol.* **2021**, *18*, 2747–2764. [[CrossRef](#)]
34. Rehman, S.; Tariq, M.; Shah, J.A.; Ahmad, R.; Shahzad, M.; Abbasi, A.M.; Ullah, A.; Ismail, B.; Bilal, M. Simultaneous physisorption and chemisorption of reactive orange 16 onto hemp stalks activated carbon: Proof from isotherm modeling. *Biointerface Res. Appl. Chem.* **2017**, *7*, 2021–2029.
35. Thivya, J.; Vijayaraghavan, J. Single and binary sorption of reactive dyes onto red seaweed-derived biochar: Multi-component isotherm and modeling. *Desalin. Water Treat.* **2019**, *156*, 87–95. [[CrossRef](#)]
36. Ivanovska, A.; Lađarević, J.; Pavun, L.; Dojčinović, B.; Cvijetić, I.; Mijin, D.; Kostić, M. Obtaining jute fabrics with enhanced sorption properties and “closing the loop” of their lifecycle. *Ind. Crop. Prod.* **2021**, *171*, 113913. [[CrossRef](#)]
37. Kheradmand, A.; Negarestani, M.; Kazemi, S.; Shayesteh, H.; Javanshir, S.; Ghiasinejad, H. Adsorption behavior of rhamnolipid modified magnetic Co/Al layered double hydroxide for the removal of cationic and anionic dyes. *Sci. Rep.* **2022**, *12*, 14623. [[CrossRef](#)]
38. Won, S.W.; Choi, S.B.; Yun, Y.-S. Performance and mechanism in binding of Reactive Orange 16 to various types of sludge. *Biochem. Eng. J.* **2006**, *28*, 208–214. [[CrossRef](#)]
39. Malek, N.N.A.; Jawad, A.H.; Ismail, K.; Razuan, R.; Al-Othman, Z.A. Fly ash modified magnetic chitosan-polyvinyl alcohol blend for reactive orange 16 dye removal: Adsorption parametric optimization. *Int. J. Biol. Macromol.* **2021**, *189*, 464–476. [[CrossRef](#)] [[PubMed](#)]
40. Abdulhameed, A.S.; Mohammad, A.-T.; Jawad, A.H. Application of response surface methodology for enhanced synthesis of chitosan tripolyphosphate/TiO<sub>2</sub> nanocomposite and adsorption of reactive orange 16 dye. *J. Clean. Prod.* **2019**, *232*, 43–56. [[CrossRef](#)]
41. Jawad, A.H.; Malek, N.N.A.; Abdulhameed, A.S.; Razuan, R. Synthesis of magnetic chitosan-fly ash/Fe<sub>3</sub>O<sub>4</sub> composite for adsorption of reactive orange 16 dye: Optimization by Box–Behnken design. *J. Polym. Environ.* **2020**, *28*, 1068–1082. [[CrossRef](#)]
42. Roy, A.; Adhikari, B.; Majumder, S.B. Equilibrium, kinetic, and thermodynamic studies of azo dye adsorption from aqueous solution by chemically modified lignocellulosic jute fiber. *Ind. Eng. Chem. Res.* **2013**, *52*, 6502–6512. [[CrossRef](#)]
43. Imessaoudene, A.; Cheikh, S.; Bollinger, J.-C.; Belkhir, L.; Tiri, A.; Bouzaza, A.; El Jery, A.; Assadi, A.; Amrane, A.; Mouni, L. Zeolite waste characterization and use as low-cost, ecofriendly, and sustainable material for malachite green and methylene blue dyes removal: Box–Behnken design, kinetics, and thermodynamics. *Appl. Sci.* **2022**, *12*, 7587. [[CrossRef](#)]
44. Rizzi, V.; Prasetyanto, E.A.; Chen, P.; Gubitosa, J.; Fini, P.; Agostiano, A.; De Cola, L.; Cosma, P. Amino grafted MCM-41 as highly efficient and reversible ecofriendly adsorbent material for the Direct Blue removal from wastewater. *J. Mol. Liq.* **2019**, *273*, 435–446. [[CrossRef](#)]
45. Srikantan, C.; Suraishkumar, G.K.; Srivastava, S. A synergistic effect of physicochemical parameters on dye removal and concomitant antioxidant production in sunflower hairy roots. *Int. J. Environ. Sci. Technol.* **2021**, *18*, 3379–3394. [[CrossRef](#)]
46. Ali, A.M.A.; Karthikeyan, R.K.; Selvan, M.S.; Rai, M.K.; Priyadharshini, M.; Maheswari, N.; Sree, G.J.; Padmanaban, V.; Singh, R.S. Removal of Reactive Orange 16 by adsorption onto activated carbon prepared from rice husk ash: Statistical modelling and adsorption kinetics. *Sep. Sci. Technol.* **2020**, *55*, 26–34. [[CrossRef](#)]
47. Ouakouak, A.; Abdelhamid, M.; Thouraya, B.; Chahinez, H.-O.; Hocine, G.; Hamdi, N.; Syafiuddin, A.; Boopathy, R. Development of a novel adsorbent prepared from dredging sediment for effective removal of dye in aqueous solutions. *Appl. Sci.* **2021**, *11*, 10722. [[CrossRef](#)]
48. Zhang, S.; Lu, X.; Liu, X.; Fang, K.; Gong, J.; Si, J.; Gao, W.; Liu, D. In situ generated UiO-66/cotton fabric easily recyclable for reactive dye adsorption. *Langmuir* **2022**, *38*, 12095–12102. [[CrossRef](#)]
49. Ivanovska, A.; Branković, I.; Lađarević, J.; Pavun, L.; Kostic, M. Oxidized jute as a valuable adsorbent for Congo Red from an aqueous solution. *J. Eng. Fiber. Fabr.* **2022**, *17*, 15589250221101380. [[CrossRef](#)]
50. Lee, C.K.; Ong, S.T.; Zainal, Z. Ethylenediamine modified rice hull as a sorbent for the removal of Basic Blue 3 and Reactive Orange 16. *Int. J. Environ. Pollut.* **2008**, *34*, 246–260. [[CrossRef](#)]
51. Mansouri, F.E.; Farissi, H.E.; Zerrouk, M.H.; Cacciola, F.; Bakkali, C.; Brigui, J.; Lovillo, M.P.; Esteves da Silva, J.C.G. Dye removal from colored textile wastewater using seeds and biochar of barley (*Hordeum vulgare* L.). *Appl. Sci.* **2021**, *11*, 5125. [[CrossRef](#)]

52. Rizzi, V.; D'Agostino, F.; Fini, P.; Semeraro, P.; Cosma, P. An interesting environmental friendly cleanup: The excellent potential of olive pomace for disperse blue adsorption/desorption from wastewater. *Dyes Pigments* **2017**, *140*, 480–490. [[CrossRef](#)]
53. Abualnaja, K.M.; Alprol, A.E.; Ashour, M.; Mansour, A.T. Influencing multi-walled carbon nanotubes for the removal of ismate violet 2r dye from wastewater: Isotherm, kinetics, and thermodynamic studies. *Appl. Sci.* **2021**, *11*, 4786. [[CrossRef](#)]

**Disclaimer/Publisher's Note:** The statements, opinions and data contained in all publications are solely those of the individual author(s) and contributor(s) and not of MDPI and/or the editor(s). MDPI and/or the editor(s) disclaim responsibility for any injury to people or property resulting from any ideas, methods, instructions or products referred to in the content.